THE JOURNAL OF PHYSICAL CHEMISTRY C

Article

pubs.acs.org/JPCC

Atomic Mechanisms and Equation of State of Methane Adsorption in Carbon Nanopores

Xueyan Zhu and Ya-Pu Zhao*

State Key Laboratory of Nonlinear Mechanics, Institute of Mechanics, Chinese Academy of Sciences, Beijing 100190, China

Supporting Information

ABSTRACT: Adsorption is an important issue both in the estimation of natural gas reserves and efficient storage of methane. In this study, we focus on the mechanisms of methane adsorption in carbon nanopores and endeavor to establish the equation of state for the adsorbed phase through molecular dynamics simulations and theoretical analyses. Here, the nanopores were modeled by carbon nanotubes (CNTs). The higher storage capacity of the CNT compared to the bulk phase was attributed to the additional pressure exerted by the CNT wall on the adsorbed phase, considering which, the equation of state for the adsorbed phase was established. As the CNT diameter increases, the adsorption structure transforms from a single-file chain to two adsorption layers. Moreover, it was found that there exists an optimal CNT diameter that maximizes the adsorption, which is due to the competition between the curvature effect and the size effect. In the explanation of this phenomenon, the nanostructure of the CNT wall plays an important role, without considering which, the adsorption density would monotonically decrease as the CNT diameter rises. Our findings and related analyses may help reveal the underlying mechanisms behind the adsorption phenomena, which is not only of theoretical importance, but may also help estimate the natural gas reserves and design nanoporous materials with higher storage capacity.

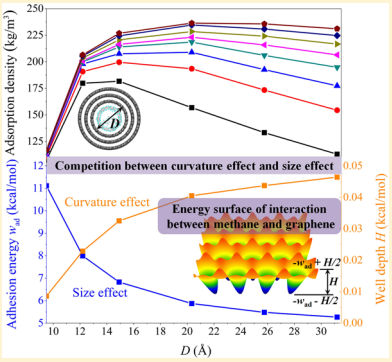

1. INTRODUCTION

With the rapid development of human society, the conventional petroleum-based and coal-based energy sources have been consumed dramatically. And due to the extensive use of these fossil fuels, the global environment has been seriously polluted. New and clean energy source should be exploited urgently for sustainable development. In this case, natural gas, the principle constituent of which is methane, is the most suitable candidate because of its low emission of carbon dioxide (CO_2) and sulfur oxide (SO_x) during combustion compared to the conventional fuel. Large amounts of natural gas are stored as adsorbed phase in the pores of shale, tight sandstones, coalbed, etc. It was found that a significant part of these pores is nanometer in scale (nanopores).[1−4] Thus, investigations on the adsorption of methane in nanopores are most important for estimating the natural gas reserves. In addition, adsorption also plays an important role in efficiently storing the natural gas. The storage of methane is an awkward problem because methane exists in the gaseous form at ambient temperature and pressure. Currently, there are three techniques for methane storage: liquefaction, compression, and adsorption. The liquefaction requires low temperature or high pressure, the condition of which is difficult to be realized in real applications. Compression of methane needs pressures as high as 20−30 MPa and the compressed phase is often stored in heavy containers to withstand high pressure, which consume lots of material and are difficult to transport. Adsorption in nanoporous materials (including carbon nanotube,[5−7] slit pore,[8−10] nanotube array,[11−13] activated carbon,[14,15] nanohorn,[16] etc.) is very efficient and promising, because it can obtain methane densities comparable to the compressed phase at much lower pressure (∼4 MPa) and ambient temperature in lightweight carriers. Therefore, the interest in exploring the adsorption phenomena in nanopores is motivated by practical considerations.

Due to the fact that the adsorption in nanopores occurs at nanoscale, atomistic simulations are needed not only for providing deep insight into the adsorption details and mechanisms but also to optimize the size and structure of the nanoporous materials for obtaining maximum storage capacity. Wilcox et al.[4] used grand canonical Monte Carlo (GCMC) simulations to estimate the adsorption isotherms of methane in slit pores with walls composited of a number of stacked graphitic layers. It was found that the excess adsorption (i.e., the density in the pore minus the bulk density) exhibits a maximum at a certain pressure and the maximum increases with the decrease of the pore size. Tan and Gubbins[8] investigated methane adsorption in carbon slit pores over a wide range of pore sizes and various supercritical temperatures. They reported that there is an optimum pore size that maximizes the excess adsorption at a given temperature and pressure. Later, Matranga, Myers, and Glandt[14] determined that a slit width of 11.4 Å is optimal for a system with a storage pressure of 3.4 MPa at ambient temperature. Gubbins et al.[17] modeled

Received: May 13, 2014
Revised: June 30, 2014
Published: July 11, 2014

   dx.doi.org/10.1021/jp5047003 | J. Phys. Chem. C 2014, 118, 17737−17744

porous carbons and zeolites to determine the best material and the optimal pore size for storing the maximum amount of methane. They found that at 274 K, the optimal material is a porous carbon of pore size sufficient to contain two adsorbed layers of methane. Cao et al.[13] investigated the adsorption behavior of methane on triangular nanotube arrays with varying tube sizes and van der Waals (vdW) gaps. Their results indicated that the optimal adsorbent with the maximum adsorption capacity at room temperature is the (15, 15) nanotube arrays with a vdW gap of 0.8 nm. Although much progress has been made, there is little concern about the underlying mechanisms of the various adsorption phenomena and no theoretical setup of the equation of state for the adsorbed phase to the best of our knowledge.

In this paper, we combined the molecular dynamics (MD) simulations and theoretical analyses to investigate methane adsorption in carbon nanotubes (CNTs), focusing on the underlying mechanisms of adsorption and endeavoring to establish the equation of state for the adsorbed phase. In section 3.1, the variations of the adsorption density and the excess adsorption with respect to the pressure and temperature from the MD results were given. And how the pore size affects the adsorption was discussed. It was found that there exists an optimal CNT diameter that maximizes the adsorption. Moreover, the adsorption structures in CNTs with different sizes were shown in section 3.2. In section 3.3, the equation of the additional pressure exerted by the CNT wall on the adsorbed phase was derived. By including the additional pressure into the equation of state for the bulk phase, the equation of state for the adsorbed phase was established. Most of the results predicted by this equation of state are in qualitative agreement with that from the MD simulations. However, this equation cannot predict the peak of the adsorption density at a certain CNT diameter due to the continuous integral and the ignorance of the nanostructure of the CNT wall. The nanostructure of the wall was considered by scanning the potential energy surface of the interaction between the methane molecule and the wall in section 3.4, which helped uncover the mechanisms for the peak of the adsorption density at a certain CNT diameter. In addition, the adsorption in carbon-based slit pores was conducted for making a comparison. The adsorption behavior in slit pore with respect to the pore size is only affected by the size effect, while the adsorption behavior in CNT is affected by both the size effect and curvature effect. How the size and curvature effects influence the adsorption was discussed in section 3.4.

2. MODEL AND METHOD

In this work, MD simulations implemented in LAMMPS[18] have been carried out for the prediction of methane adsorption in CNTs. Due to the physisorption nature of methane adsorption in CNTs,[19] the fundamental interacting energy between methane and the CNT is caused by van der Waals interactions. Thus, methane atoms and carbon atoms were modeled as Lennard-Jones (LJ) particles. The LJ cutoff was set to be 10 Å. The LJ parameters came from the consistent valence force-field (cvff),[20] which is based on the experimental values and ab initio calculations. The interactions between methane atoms and carbon atoms were calculated by the Lorentz−Berthelot (LB) rule.

The adsorption model was established as shown in Figure 1. The CNT was fixed during the whole process and connected with the bulk phase of methane. We set walls between the bulk phase and the CNT to make sure that the methane molecules can only adsorb on the inner wall of the CNT. Initially, there were no methane molecules in the CNT. Under the constant pressure provided by the bulk phase, the methane molecules entered into the CNT. Then, due to the intermolecular interactions between methane molecules and the CNT, methane molecules that have entered into the CNT were adsorbed on the CNT wall. The whole system was modeled in NVT ensemble with Nose/Hoover method and the time step was 1 fs. However, the adsorbed methane in CNT was actually in grand canonical (μVT) ensemble because the chemical potential and temperature of methane in CNT are equal to those of the bulk phase in equilibrium. Five CNTs [(7, 7), (9, 9), (11, 11), (15, 15), (19, 19), (23, 23)] with diameters varying from 9 to 32 Å were chosen to explore the effect of the pore size on the adsorption behavior. The adsorption processes were modeled at temperatures of 300, 340, and 380 K, and pressures in the range of 20−300 bar. It should be emphasized that the pressure was controlled by the density of the bulk phase. For every state, the total simulation time was 3000 ps. The former 1000 ps was used for reaching equilibrium, whereas the latter 2000 ps for data acquisition.

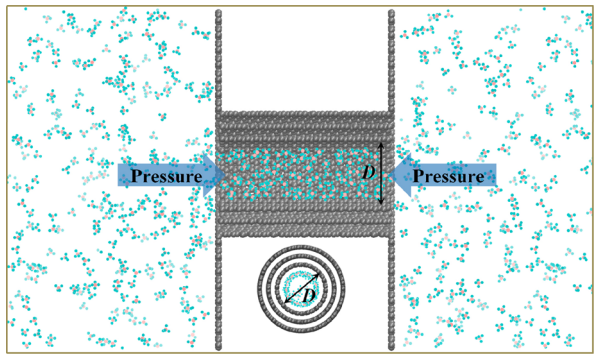

Figure 1. Visualization of the MD simulation domain. The inset shows the cross section of the CNT.

3. RESULTS AND DISCUSSION

3.1. Adsorption Density as a Function of Pressure, Temperature, and Pore Size. To examine the effect of pressure and temperature on the adsorption amount of methane in CNT, we plotted the isotherms of the adsorption density in Figure 2a. The adsorption density is just the density of methane in the CNT which is calculated by dividing the total mass of methane in the CNT by the inner volume of the CNT. As pressure increases, the adsorption density increases and tends to saturation at high pressure. The increase in temperature leads to the decrease of the adsorption density.

By making a comparison between the adsorbed and bulk phase, it was found that at the same temperature and pressure the adsorption density is larger than the bulk density as shown in Figure 2a. This indicates that the nanopore has the capability of storing more methane than the bulk phase. Taking the (15, 15) CNT for an example, the CNT can contain 10 times more methane than the bulk phase in an equivalent volume at T = 300 K and p = 20 bar. From another perspective, the amount of methane molecules that can be stored in CNT at 20 bar is as much as that in the bulk phase at 220 bar. This phenomenon is attributed to the additional pressure exerted by the CNT on the adsorbed phase. In section 3.3, we would derive the equation

dx.doi.org/10.1021/jp5047003 | J. Phys. Chem. C 2014, 118, 17737−17744

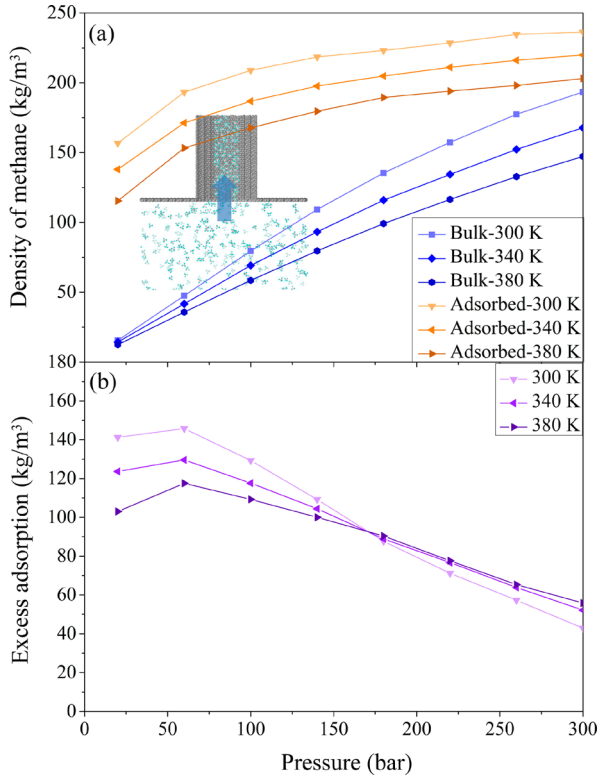

Figure 2. (a) Isotherms of the adsorption density (orange line) in (15, 15) CNT and the bulk density (blue line), respectively. (b) Isotherms of the excess adsorption, which is the difference between the adsorption density and the bulk density.

for calculating this additional pressure and add it to the equation of state.

The difference between the adsorption density ρ_{ad} and the bulk density ρ_{bulk} was defined as the excess adsorption

$$\Gamma = \rho_{ad} - \rho_{bulk} \quad (1)$$

The isotherms of the excess adsorption were plotted in Figure 2b. With the increase in pressure, the excess adsorption increases up to a maximum value at 60 bar, and then decreases, which suggests an optimum pressure for maximum methane storage. This can be explained below. First, in the limiting case of zero pressure, the bulk density, and adsorption density should both be zero, which leads to the zero excess adsorption. Second, accompanying with the pressure being increased to be nonzero, methane molecules quickly adsorb onto the empty adsorption sites distributed on the CNT wall. In this case, the adsorption density is larger than the bulk density due to the additional pressure exerted by the CNT on the adsorbed phase, thus leading to positive excess adsorption. As pressure continues to increase, the methane molecules fill up the available adsorption sites, until there is little room for accommodating much more methane molecules into the CNT, at which point the increase gradient of the adsorption density with respect to the pressure becomes smaller than that of the bulk density. This indicates quicker saturation of the adsorbed phase and leads to the decrease of the excess adsorption. Third, with sufficient pressure increase, the bulk density increases to be equal to the adsorption density, at which point the excess adsorption becomes zero again. Therefore, the excess adsorption first increases ($\partial\Gamma/\partial p > 0$), then decreases ($\partial\Gamma/\partial p < 0$) as pressure rises.

Figure 2a showed that $\partial\rho_{ad}/\partial T \approx$ const, while $\partial\rho_{bulk}/\partial T$ decreases with the increase of pressure. Thus, the temperature gradient of the excess adsorption, which is $\partial\Gamma/\partial T = \partial\rho_{ad}/\partial T - \partial\rho_{bulk}/\partial T$, increases with the increase of the pressure. Considering $\partial\rho_{ad}/\partial T < \partial\rho_{bulk}/\partial T$ at 20 bar, $\partial\Gamma/\partial T$ is negative initially, then increases to zero with the increase of the pressure to a critical value, above which $\partial\Gamma/\partial T > 0$. This corresponds to the phenomena present in Figure 2b that the excess adsorption decreases with the increase of the temperature in the low pressure region (p < 170 bar), while it increases with the temperature in the high pressure region (p > 170 bar). Moreover, increased temperature causes a lower peak in the excess adsorption. The data of the excess adsorption also show that the storage capacity of the CNT can exceed the target of the U.S. Department of Energy,[15] 150 V/V (i.e., 97 kg/m^3) in the low pressure region.

Further insight was gain into how the pore size influences the adsorption. Figure 3a shows the variation of the adsorption

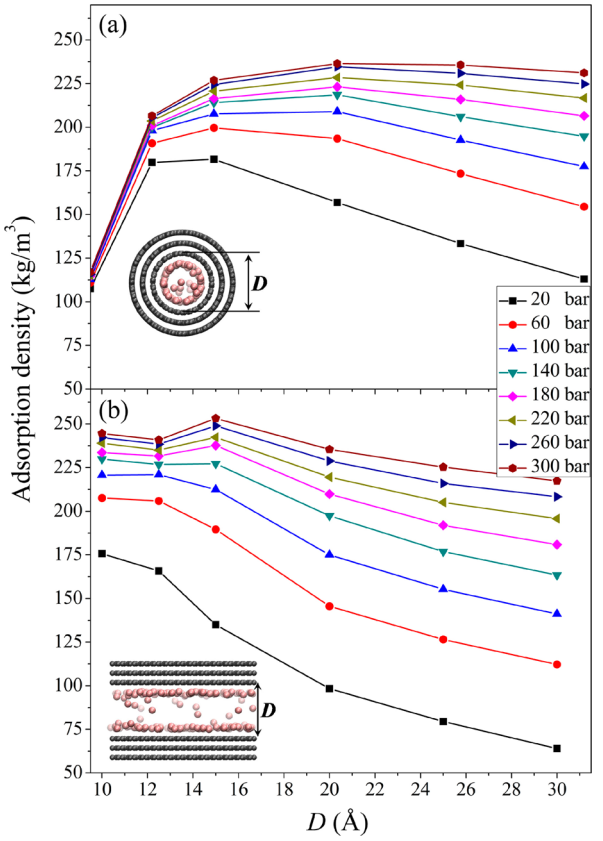

Figure 3. Adsorption density in CNT (a) and carbon-based slit pore (b) as a function of the pore size D at 300 K and pressures ranging from 20 to 300 bar.

density as a function of the CNT diameter. Interestingly, with the increase of the CNT diameter, the adsorption density increases up to a maximum value, and then decreases, which indicates the existence of an optimum size of the CNT for maximum methane storage. For p = 20−60 bar, the optimum size is 14.92 Å, while for p = 100−300 bar, the optimum size is 20.34 Å. Thus, the optimum size tends to increase as the pressure rises. Moreover, it was found that the increase gradient before the optimum size is much larger than the decrease gradient after the optimum size. And with the increase in pressure, the increase gradient increases, while the decrease

dx.doi.org/10.1021/jp5047003 | J. Phys. Chem. C 2014, 118, 17737−17744

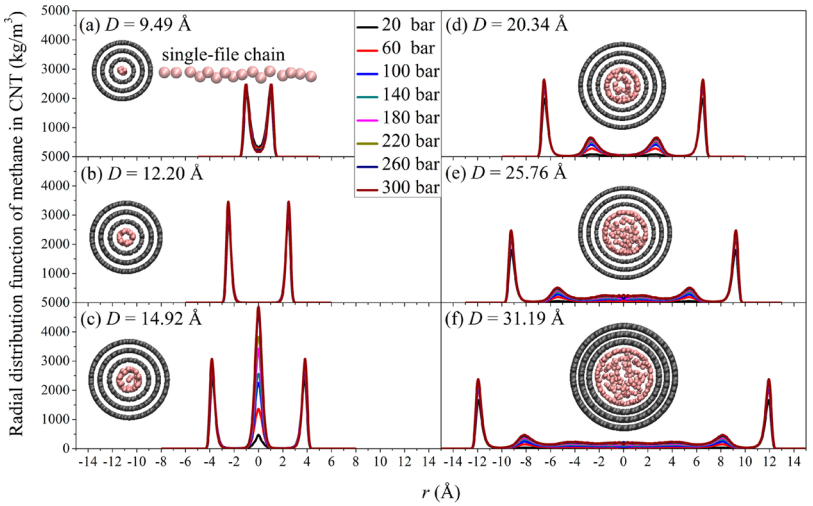

Figure 4. RDFs of methane in the six CNTs with diameters D from 9.49 to 31.19 Å. The insets show the corresponding snapshots of the adsorption structures from the simulations (T = 300 K). (a) D = 9.49 Å. Methane molecules form a single-file chain in the CNT. (b) D = 12.20 Å. The CNT allows for the formation of one adsorption layer. (c) D = 14.92 Å. The CNT creates additional space in the CNT center for the formation of a single-file chain. (d) D = 20.34 Å. Two adsorption layers form. (e and f) D = 25.76−31.19 Å. A central layer forms, whose density is identical to the bulk phase.

gradient decreases. In addition, we plotted the variation of the adsorption density in slit pores as a function of the pore size (Figure 3b) for making a comparison, which is discussed in section 3.4 to uncover how the size effect and curvature effect influence the adsorption, respectively.

We would like to compare our MD results with the experimental results in the literature here. The isotherms from the experiments[21,22] show that the adsorption density increases with the increase of the pressure and tends to saturation at high pressure. The experimental data also found the decrease of the adsorption density as temperature rises. These results are in agreement with the above discussions. Then, the conditions of T = 300 K, p = 20 bar and T = 300 K, p = 100 bar were chosen to compare the adsorption data from our MD simulations with that from the experiments. Lee et al.[21] fabricated CNTs with diameters of 40−60 nm and determined the amount of adsorbed methane about 1.48 mmol/g at 303.15 K and 19.48 bar. Rasoolzadeh et al.[22] studied methane adsorption in CNTs with diameter of about 5 nm at 298 K and 20 bar and achieved the adsorption capacity of about 1.2 mmol/g. In this work, an adsorption capacity of 2.17 mmol/g for a 3 nm sized CNT was obtained under similar conditions of 300 K and 20 bar. At approximate 300 K and 100 bar, Wu et al.[23] reported total amount of adsorbed methane about 1.8 mmol/g in CNTs with diameters of 5−8 nm, while our work predicted adsorption capacity of 3.40 mmol/g in 3 nm sized CNT. The adsorption capacity from our MD simulations is of the same order of that from the experiments under similar conditions, but a little larger than that achieved by the experiments. This may be due to the smaller CNT used in our simulations than in the experiments. The comparison with experiments illustrated that our MD results are reasonable.

3.2. Adsorption Structures from a Single-File Chain to Two Adsorption Layers. To explore the adsorption structures and density distributions of methane in CNTs, we plotted the radial distribution function (RDF) of methane along the radial direction in Figure 4. The term r represents the distance from the CNT center. The section for r < 0 was plotted as the mirror of the section for r > 0 to reflect the symmetrical distribution of methane with respect to the CNT center. Generally, as the CNT diameter increases, the peaks of the RDF first increase and then decrease, which is consistent with the existence of an optimal CNT diameter for maximum methane storage discussed above. All the RDF peaks increase with the increase in pressure. Moreover, the density of the layer at the wall outstrips 1000 kg/m^3, which indicates the densification of the first adsorption layer due to the confinement effect.

The adsorbed methane exhibits different structures in CNTs with different diameters. For D = 9.49 Å, the methane molecules form a single-file chain encapsulated by the CNT as shown in the inset of Figure 4a. However, the RDFs in this case do not exhibit a single peak in the CNT center as expected, but two symmetrical peaks. This is because the methane molecules of the single-file chain do not exactly stay in the CNT center, but around the center, and are in zigzag arrangement. This kind of arrangement can help the CNT store more methane molecules than the exactly linear arrangement. The 12.20 Å sized CNT allows for the formation of one adsorption layer as indicated by the RDFs in Figure 4b. When D further increases to 14.92 Å, the CNT creates additional space in the center for the formation of a central single-file chain (Figure 4c). As pressure rises, the density of the central single-file chain increases greatly, while there is only slight increase of the density of the layer at the wall. This illustrates that the methane molecules tend to preferentially occupy the adsorption sites at the wall, then the central region. For D = 20.34−31.19 Å, two adsorption layers form as indicated by the two peaks nearest to the CNT wall (Figure 4d−f). With the increase in pressure, the density of the second layer increases rapidly, while the density of the first layer rises slowly. In the case of D = 25.76−31.19 Å (Figure 4e and f), there is another clear pattern that a central layer forms, whose density is identical to the bulk phase. This indicates that the central region, whose distance from the wall is approximately 7 Å, is out of the range of the confinement of the wall.

3.3. Equation of State for the Adsorbed Phase. In this section, we would explore the adsorption of methane in CNT

dx.doi.org/10.1021/jp5047003 | J. Phys. Chem. C 2014, 118, 17737−17744

theoretically. As we have mentioned above, the adsorbed phase bears additional pressure due to the attractive interactions between the adsorbed methane molecules and the CNT. The interaction energy between a methane molecule and a carbon atom was modeled by the LJ potential:

$$u_0(\rho) = 4\varepsilon\left[\left(\frac{\sigma}{\rho}\right)^{12} - \left(\frac{\sigma}{\rho}\right)^{6}\right] \tag{2}$$

where ε = 0.22 kcal/mol is the potential well depth, σ = 3.59 Å is the distance at which the LJ potential is zero, and ρ is the distance between the methane molecule and the carbon atom. The integral of eq 2 over the whole volume of the CNT yields the interaction energy between a methane molecule and the CNT[24]

$$\begin{aligned} w_0(r) &= \rho_{cnt}\int_{-\infty}^{\infty}\int_0^{2\pi}\int_{R_0}^{\infty} u_0(\rho) r_1\, dr_1\, d\theta\, dz \\ &= \pi^2\rho_{cnt}\varepsilon\sigma^3\left\{\frac{7\sigma^9}{32{R_0}^9}F\left[\frac{9}{2}, \frac{11}{2}; 1; \left(\frac{r}{R_0}\right)^2\right]\right. \\ &\quad \left. - \frac{\sigma^3}{{R_0}^3}F\left[\frac{3}{2}, \frac{5}{2}; 1; \left(\frac{r}{R_0}\right)^2\right]\right\} \end{aligned} \tag{3}$$

with

$$\rho^2 = r^2 + {r_1}^2 - 2rr_1\cos\theta + z^2 \tag{4}$$

In eq 3, ρ_{cnt} is the number density of the CNT, $R_0 = D/2$ is the radius of the CNT, r is the radial coordinate of the methane molecule, and F is the hypergeometric function, which is defined by the power series

$$F(a, b; c; z) = \sum_{n=0}^{\infty}\frac{(a)_n(b)_n}{(c)_n}\frac{z^n}{n!} \tag{5}$$

with the Pochhammer symbols $(a)_n$, $(b)_n$, and $(c)_n$ defined by

$$(q)_n = \begin{cases} 1 & (n = 0) \\ q(q+1)\cdots(q+n-1) & (n > 0) \end{cases} \tag{6}$$

Assuming that the density of the adsorbed phase uniformly distributes throughout the CNT, the interaction energy between the adsorbed phase and the CNT per unit area was obtained

$$\begin{aligned} W(R_0, r) &= \rho_{av}\int_0^r w_0(r')(r'/r)\, dr' \\ &= \frac{\pi R_0\rho_{cnt}\rho_{av}\varepsilon\sigma^6}{720r(r-R_0)^8(r+R_0)^8}\left[f_1(R_0, r)E\left(\frac{r^2}{{R_0}^2}\right)\right. \\ &\quad \left. - f_2(R_0, r)K\left(\frac{r^2}{{R_0}^2}\right)\right] \end{aligned} \tag{7}$$

with

$$\begin{aligned} f_1(R_0, r) &= -480(r^2-{R_0}^2)^6(r^2+{R_0}^2) + (5r^8 + 428r^6{R_0}^2 \\ &\quad + 1182r^4{R_0}^4 + 428r^2{R_0}^6 + 5{R_0}^8)\sigma^6 \\ f_2(R_0, r) &= 480(r^2-{R_0}^2)^7 - (r^2-{R_0}^2)(155r^6 + 591r^4{R_0}^2 \\ &\quad + 273r^2{R_0}^4 + 5{R_0}^6)\sigma^6 \end{aligned} \tag{8}$$

in which ρ_{av} is the average number density of the adsorbed phase over the radial coordinate from 0 to r, E is the complete elliptic integral of the second kind, and K is the complete elliptic integral of the first kind. The differential of W with respect to r produces the additional pressure exerted by the CNT

$$\begin{aligned} \prod(R_0, r) &= -\frac{dW}{dr} \\ &= \frac{\pi R_0\rho_{cnt}\rho_{av}\varepsilon\sigma^6}{720r^2(r^2-{R_0}^2)^9}\left[g_1(R_0, r)E\left(\frac{r^2}{{R_0}^2}\right)\right. \\ &\quad \left. - g_2(R_0, r)K\left(\frac{r^2}{{R_0}^2}\right)\right] \end{aligned} \tag{9}$$

with

$$\begin{aligned} g_1(R_0, r) &= -960r^{16} + 2400r^{14}{R_0}^2 + 6240r^{12}{R_0}^4 \\ &\quad + 5{R_0}^{10}(96{R_0}^6 - \sigma^6) - 40r^{10}(852{R_0}^6 - \sigma^6) \\ &\quad + 2r^4{R_0}^6(13200{R_0}^6 + 5201\sigma^6) \\ &\quad + 25r^8(2400{R_0}^8 + 179{R_0}^2\sigma^6) \\ &\quad + r^6(-54240{R_0}^{10} + 17188{R_0}^4\sigma^6) \\ &\quad + r^2(-6240{R_0}^{14} + 668{R_0}^8\sigma^6) \\ g_2(R_0, r) &= (r^2-{R_0}^2)[2400r^{14} - 14880r^{12}{R_0}^2 \\ &\quad + 38880r^{10}{R_0}^4 + 5{R_0}^8(-96{R_0}^6 + \sigma^6) \\ &\quad - 5r^8(11040{R_0}^6 + 311\sigma^6) \\ &\quad - 6r^4{R_0}^4(3600{R_0}^6 + 1031\sigma^6) \\ &\quad + 20r^6(2280{R_0}^8 - 407{R_0}^2\sigma^6) \\ &\quad + r^2(5280{R_0}^{12} - 508{R_0}^6\sigma^6)] \end{aligned} \tag{10}$$

Based on the Peng–Robinson equation of state for the bulk phase[25]

$$\begin{aligned} p &= \frac{RT}{V_m - b} - \frac{a\alpha}{{V_m}^2 + 2bV_m - b^2} \\ a &= \frac{0.457235R^2{T_c}^2}{p_c},\ b = \frac{0.077796RT_c}{p_c},\ T_r = \frac{T}{T_c} \\ \alpha &= [1 + \kappa(1 - T_r^{0.5})]^2, \\ \kappa &= 0.37464 + 1.54226\omega - 0.26992\omega^2 \end{aligned} \tag{11}$$

in which, V_m is the molar volume, R is the ideal gas constant, T_c is the critical temperature, p_c is the critical pressure, and ω is the acentric factor, the equation of state for the adsorbed phase was proposed as

$$\begin{aligned} &\chi_p\left(\frac{p}{p_c}\right)^{\Delta_p}p_c + \chi_\prod\prod(R_0, r) \\ &= \chi_T\frac{RT_c(T/T_c)^{\Delta_T}}{(N_A/\rho_{av}) - b} - \frac{a\alpha}{(N_A/\rho_{av})^2 + 2b(N_A/\rho_{av}) - b^2} \end{aligned} \tag{12}$$

where N_A is the Avogadro's constant, χ_p, $\chi_\prod$, χ_T, Δ_p, and Δ_T are nondimensional constants that can be tuned empirically. Based on the adsorption density of the (15, 15) CNT from MD results, these five nondimensional constants were obtained to be χ_p = 2.68, $\chi_\prod$ = 0.10, χ_T = 1.39, Δ_p = 0.23, and Δ_T = 0.21. It

dx.doi.org/10.1021/jp5047003 | J. Phys. Chem. C 2014, 118, 17737–17744

should be emphasized that ρ_{av} obtained from eq 12 is the average density over the radial coordinate from 0 to r. The variation of ρ_{av} with respect to r at 300 K and 20 bar in (15, 15) CNT was plotted in Figure 5a. ρ_{av} near the wall is much larger

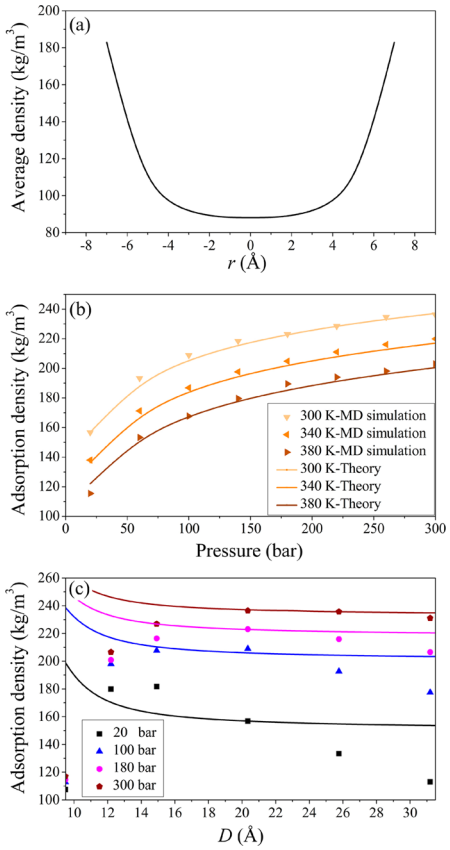

Figure 5. Adsorption phenomena predicted by the equation of state for the adsorbed phase (eq 12). (a) The variation of the average adsorption density with respect to the radial coordinate r. (b) Isotherms of the adsorption density in (15, 15) CNT from MD simulations (points) and eq 12 (lines). (c) Adsorption density as a function of the CNT diameter D from MD simulations (points) and eq 12 (lines), respectively.

than ρ_{av} in the center of the CNT, which is in qualitative agreement with MD results (Figure 4d). Through statistics of the equilibrium states from the simulations, the average equilibrium distance between the first adsorption layer and the inner wall of the CNT was obtained to be h_e = 3.70 Å. Thus, the adsorption density should be the average density over the radial coordinate from 0 to $r_{eq} = R_0 - h_e$, i.e., ρ_{av} when $r = r_{eq}$.

The adsorption density obtained from eq 12 was plotted in Figure 5 as a function of temperature, pressure, and the CNT diameter. The isotherms of adsorption density in (15, 15) CNT predicted by eq 12 is in quantitative agreement with that from the MD results (Figure 5b). The comparisons between the isotherms from eq 12 and the isotherms from MD for adsorption in CNTs with different diameters were shown in Supporting Information 1. With the increase in the CNT diameter, eq 12 predicts the monotonous decrease of the adsorption density (Figure 5c), which disagrees with the peak of the adsorption density at a certain CNT diameter (Figure 3a) from the MD results. This is because eq 12 is established based on the continuous integral, thus ignoring the nanostructure of the CNT wall, which would be discussed in the next section. Figure 5c also shows that the theory is in more agreement with the MD results in the CNTs with larger diameters and at higher pressures.

3.4. Curvature Effect versus Size Effect. Why does the adsorption density peak at a certain CNT diameter? To address this question, the nanostructure of the CNT wall should be considered. The potential energy surface of the interaction between a methane molecule and the wall was scanned at h_e as shown in Figure 6. It was found that the energy surface is not a

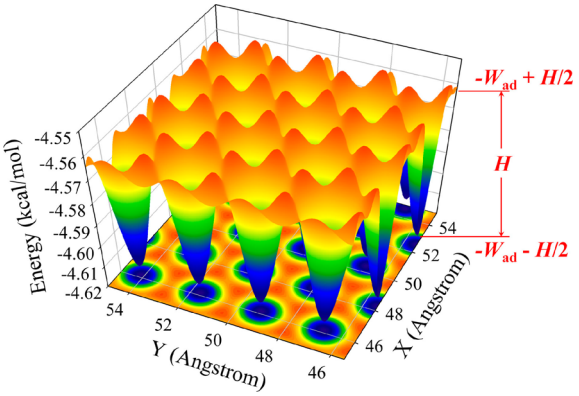

Figure 6. Potential energy surface of the interaction between a methane molecule and the CNT wall.

plane, but a curved surface with periodic ridges and valleys due to the nanostructure of the wall. The energy surface is characterized by two variables: one is the average interaction energy, the negative value of which is just the adhesion energy W_{ad}; and the other is the well depth H, which determines the energy difference between the ridges and valleys. With larger adhesion energy and well depth, the methane molecule should be bound stronger to the wall, which can enhance the adsorption capacity of the pore, thus leading to larger adsorption density. The adhesion energy and the well depth vary as a function of the CNT diameter as shown in Figure 7a. With the increase of D, the distance between the adsorbed methane molecule and the CNT atoms becomes larger, thus,

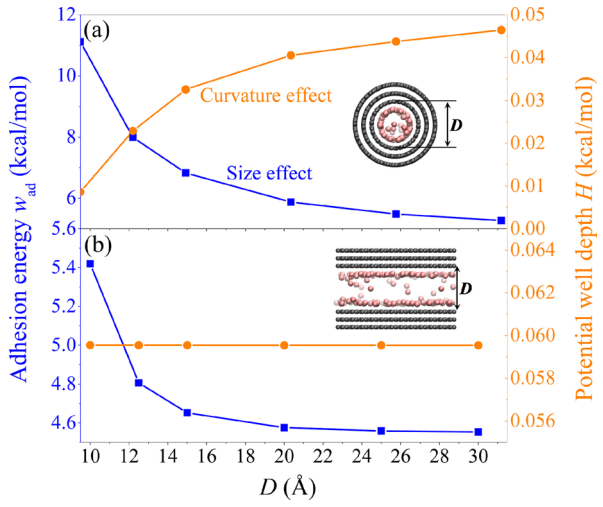

Figure 7. Variation of the adhesion energy (■) and the potential well depth (●) with respect to the pore size D for the (a) CNT and (b) slit pore, respectively.

dx.doi.org/10.1021/jp5047003 | J. Phys. Chem. C 2014, 118, 17737−17744

leading to weaker van der Waals interactions. This indicates that the energy required for removing a methane molecule from the CNT wall becomes smaller as D rises. Therefore, the adhesion energy decreases with D. However, the well depth increases with the increase of D. This leads to the opposite variation trends of the adsorption density with respect to D, which explains the peak of the adsorption density at a certain D. Therefore, the mechanisms for the peak of the adsorption density should be the competition between the inverse variation trends of the adhesion energy and the well depth with respect to D.

It was noticed that with the decrease of the CNT diameter, not only is the CNT size decreasing, but the CNT curvature is increasing. Thus, there are two factors that affect the adsorption, i. e., the size effect and the curvature effect. To explore how these two factors affect the adsorption and decouple these two factors, we conducted another simulation of the adsorption in carbon-based slit pores at 300 K. In this simulation, the curvature effect is eliminated, leaving only the size effect, because the curvature of the graphite is always zero. As shown in Figure 3b, when $p < 180$ bar, the adsorption density monotonically decreases as D rises and does not exhibit a peak. When $p \geq 180$ bar, the adsorption density peaks at $D = 15$ Å. This indicates that the adsorption exhibits different behaviors in the low pressure region and in the high pressure region. In the low pressure region, the adsorption has not saturated, thus, mainly depends on the interactions between methane molecules and the wall. The potential energy surface of the interaction between a methane molecule and the wall of the slit pore was scanned at h_e was scanned. As shown in Figure 7b, the adhesion energy decreases with D, but the well depth remains almost unchanged. This leads to the monotonous decrease of the adsorption density with D in the low pressure region. However, as pressure rises, the adsorption density in smaller pores saturates more quickly than that in larger pores. Thus, when the pressure is high enough, the adsorption density in larger pores would exceed that in smaller pores. This explains the peak of the adsorption density at a certain pore size in the high pressure region.

The above discussions illustrated that the variation trend of the adhesion energy with D is the same for the CNT and the slit pore, while the well depth increases with D in CNT, but remains almost unchanged in the slit pore (Figure 7). This suggests that the increase of the well depth with D in the CNT is controlled by the curvature effect, but the decrease of the adhesion energy with D is mainly controlled by the size effect. From another perspective, the decrease of the size, i.e., the decrease of D, leads to the increase of the adhesion energy, while the decrease of the curvature, i.e., the increase of D, leads to the increase of the well depth. Therefore, the existence of the optimal CNT size for maximum methane storage is due to the competition between the size effect and the curvature effect.

4. CONCLUSIONS

Employing MD simulations and theoretical analyses, various methane adsorption phenomena in CNT were reported and the underlying mechanisms were uncovered. The CNT can store much more methane than the bulk phase at the same temperature and pressure. And there exists an optimal CNT diameter that maximizes the adsorption. With the increase of the diameter, the adsorption structure transforms from a single-file chain to two adsorption layers. These phenomena were attributed to the additional pressure exerted by the CNT wall on the adsorbed phase. By including the additional pressure into the equation of state for the bulk phase, the equation of state for the adsorbed phase was established. This equation can predict most of the adsorption phenomena found in the simulations. However, it cannot predict the peak of the adsorption density at a certain CNT diameter due to the ignorance of the nanostructure of the CNT wall. To explain this phenomenon, the potential energy surface of the interaction between the methane molecule and the CNT wall was scanned. The energy surface is a curved surface with periodic ridges and valleys due to the nanostructure of the wall, which is characterized by the adhesion energy and the well depth. With the change of the CNT diameter, the adhesion energy and the well depth show inverse variation trends, thus leading to the peak of the adsorption density. Moreover, the adsorption in slit pore was conducted for making a comparison. The adsorption behavior in slit pore with respect to the pore size is only affected by the size effect, while the adsorption behavior in CNT affected by both the size and curvature effects. It was found that the variation of the adhesion energy with respect to the pore size is mainly controlled by the size effect, but the well depth by the curvature effect. Thus, the peak of the adsorption density is also attributed to the competition between the size effect and the curvature effect.

■ ASSOCIATED CONTENT

Supporting Information

Detailed comparison between MD results and theoretical predictions including Figures S1−S4. This material is available free of charge via the Internet at http://pubs.acs.org.

■ AUTHOR INFORMATION

Corresponding Author

*E-mail: yzhao@imech.ac.cn.

Notes

The authors declare no competing financial interest.

■ ACKNOWLEDGMENTS

This work was jointly supported by the National Natural Science Foundation of China (NSFC, grant no. 11372313), the Key Research Program of the Chinese Academy of Sciences (grant no. KJZD-EW-M01), and the Instrument Developing Project of the Chinese Academy of Sciences (grant no. Y2010031).

■ REFERENCES

(1) Gan, H.; Nandi, S. P.; Walker, P. L., Jr Nature of the Porosity in American Coals. *Fuel* **1972**, *51*, 272−277.

(2) Mardon, S. M. Evaluation of Coalbed Methane and Carbon Dioxide Sequestration Potential in the Western Kentucky Coalfield. M.S. Thesis, University of Kentucky, 2008.

(3) Loucks, R. G.; Reed, R. M.; Ruppel, S. C.; Jarvie, D. M. Morphology, Genesis, and Distribution of Nanometer-Scale Pores in Siliceous Mudstones of the Mississippian Barnett Shale. *J. Sediment. Res.* **2009**, *79*, 848−861.

(4) Mosher, K.; He, J. J.; Liu, Y. Y.; Rupp, E.; Wilcox, J. Molecular Simulation of Methane Adsorption in Micro- and Mesoporous Carbons with Applications to Coal and Gas Shale Systems. *Int. J. Coal Geol.* **2013**, *109*, 36−44.

(5) Muris, M.; Dufau, N.; Bienfait, M.; Dupont-Pavlovsky, N.; Grillet, Y.; Palmari, J. P. Methane and Krypton Adsorption on Single-Walled Carbon Nanotubes. *Langmuir* **2000**, *16*, 7019−7022.

(6) Tanaka, H.; El-Merraoui, M.; Steele, W. A.; Kaneko, K. Methane Adsorption on Single-Walled Carbon Nanotube: A Density Functional Theory Model. *Chem. Phys. Lett.* **2002**, *352*, 334−341.
(7) Cao, D. P.; Wu, J. Z. Self-Diffusion of Methane in Single-Walled Carbon Nanotubes at Sub- and Supercritical Conditions. *Langmuir* **2004**, *20*, 3759−3765.
(8) Tan, Z. M.; Gubbins, K. E. Adsorption in Carbon Micropores at Supercritical Temperatures. *J. Phys. Chem.* **1990**, *94*, 6061−6069.
(9) Kowalczyk, P.; Tanaka, H.; Kaneko, K.; Terzyk, A. P.; Do, D. D. Grand Canonical Monte Carlo Simulation Study of Methane Adsorption at an Open Graphite Surface and in Slitlike Carbon Pores at 273 K. *Langmuir* **2005**, *21*, 5639−5646.
(10) Yeganegi, S.; Gholampour, F. Methane Adsorption and Diffusion in a Model Nanoporous Carbon: An Atomistic Simulation Study. *Adsorpt.-J. Int. Adsorpt. Soc.* **2013**, *19*, 979−987.
(11) Talapatra, S.; Zambano, A. Z.; Weber, S. E.; Migone, A. D. Gases Do Not Adsorb on the Interstitial Channels of Closed-Ended Single-Walled Carbon Nanotube Bundles. *Phys. Rev. Lett.* **2000**, *85*, 138−141.
(12) Talapatra, S.; Migone, A. D. Adsorption of methane on bundles of closed-ended single-wall carbon nanotubes. *Phys. Rev. B* **2002**, *65*, 045416.
(13) Cao, D. P.; Zhang, X. R.; Chen, J. F.; Wang, W. C.; Yun, J. Optimization of Single-Walled Carbon Nanotube Arrays for Methane Storage at Room Temperature. *J. Phys. Chem. B* **2003**, *107*, 13286−13292.
(14) Matranga, K. R.; Myers, A. L.; Glandt, E. D. Storage of Natural Gas by Adsorption on Activated Carbon. *Chem. Eng. Sci.* **1992**, *47*, 1569−1579.
(15) Lozano-Castello, D.; Cazorla-Amoros, D.; Linares-Solano, A. Powdered Activated Carbons and Activated Carbon Fibers for Methane Storage: A Comparative Study. *Energy Fuels* **2002**, *16*, 1321−1328.
(16) Ohba, T.; Kaneko, K.; Yudasaka, M.; Iijima, S.; Takase, A.; Kanoh, H. Cooperative Adsorption of Supercritical CH_4 in Single-Walled Carbon Nanohorns for Compensation of Nanopore Potential. *J. Phys. Chem. C* **2012**, *116*, 21870−21873.
(17) Cracknell, R. F.; Gordon, P.; Gubbins, K. E. Influence of Pore Geometry on the Design of Microporous Materials for Methane Storage. *J. Phys. Chem.* **1993**, *97*, 494−499.
(18) Plimpton, S. Fast Parallel Algorithms for Short-Range Molecular Dynamics. *J. Comput. Phys.* **1995**, *117*, 1−19.
(19) Delavar, M.; Ghoreyshi, A. A.; Jahanshahi, M.; Khalili, S.; Nabian, N. Equilibria and Kinetics of Natural Gas Adsorption on Multi-Walled Carbon Nanotube Material. *RSC Adv.* **2012**, *2*, 4490−4497.
(20) Dauber-Osguthorpe, P.; Roberts, V. A.; Osguthorpe, D. J.; Wolff, J.; Genest, M.; Hagler, A. T. Structure and Energetics of Ligand Binding to Proteins: Escherichia Coli Dihydrofolate Reductase-Trimethoprim, a Drug-Receptor System. *Proteins* **1988**, *4*, 31−47.
(21) Lee, J. W.; Kang, H. C.; Shim, W. G.; Kim, C.; Moon, H. Methane Adsorption on Multi-Walled Carbon Nanotube at (303.15, 313.15, and 323.15) K. *J. Chem. Eng. Data* **2006**, *51*, 963−967.
(22) Rasoolzadeh, M.; Fatemi, S.; Gholamhosseini, M.; Moosaviyan, M. A. Study of Methane Storage and Adsorption Equilibria in Multi-Walled Carbon Nanotubes. *Iran. J. Chem. Chem. Eng.* **2008**, *27*, 127−134.
(23) Wu, Y. L.; Wei, F.; Luo, G. H.; Ning, G. Q.; Yang, M. D. Methane Storage in Multi-Walled Carbon Nanotubes at the Quantity of 80 g. *Mater. Res. Bull.* **2008**, *43*, 1431−1439.
(24) Philip, J. R. Adsorption and Geometry: The Boundary Layer Approximation. *J. Chem. Phys.* **1977**, *67*, 1732−1741.
(25) Peng, D.-Y.; Robinson, D. B. A New Two-Constant Equation of State. *Ind. Eng. Chem. Fundam.* **1976**, *15*, 59−64.